J Appl Electrochem (2011) 41:623–631
DOI 10.1007/s10800-011-0271-6

ORIGINAL PAPER

Bench-scale electrochemical system for generation of CO and syn-gas

Eric J. Dufek · Tedd E. Lister · Michael E. McIlwain

Received: 15 November 2010 / Accepted: 17 February 2011 / Published online: 2 March 2011

Abstract A flow cell based, bench-scale electrochemical system for generation of synthesis-gas (syn-gas) is reported. Sensitivity to operating conditions such as CO_2 flow, current density, and elevated temperature are described. By increasing the temperature of the cell the kinetic overpotential for the reduction of CO_2 was lowered with the cathode voltage at 70 mA cm^{-2} decreased by 0.32 V and the overall cell voltage dropping by 1.57 V. This equates to an 18% increase in cell efficiency. By closely monitoring the products it was found that at room temperature and 70 °C the primary products are CO and H_2. By controlling the current density and the flow of CO_2 it was possible to control the H_2:CO product ratio between 1:4 and 9:1. The reproducibility of performing experiments at elevated temperature and the ability to generate syn-gas for extended periods of time is also discussed.

Keywords Carbon dioxide reduction · Gas diffusion electrode · Syn-gas · Energy storage · Energy conversion · Electrolysis · Load-leveling

1 Introduction

The production of sustainable transportation fuels has become a priority for continued human prosperity. While hydrogen is a possibility, several issues remain to make it a viable option. The production of either CO or synthesis-gas (syn-gas), a combination of CO and H_2, electrochemically from CO_2 and H_2O is an alternative to hydrogen. From syn-gas, generation of hydrocarbon fuels has the potential to produce carbon neutral products that can be used in the existing transportation infrastructure with minimal modifications [1]. Unfortunately, the electrochemical reduction of CO_2 is hindered by issues with low energy efficiency due to kinetic limitations [2, 3]. In economic terms, inefficiencies may be less of an issue as alternative electrical sources such as wind and solar are introduced to the electrical grid. These sources of electricity tend to be highly variable and will require load-leveling technology either in the form of energy storage or conversion to fully realize their economic value. Thus, generating hydrocarbon products from CO_2 provides a means to enhance load-leveling capabilities for emerging energy systems. This work aims to explore the use of a flow cell configuration which incorporates materials and chemical conditions which have proven effective at syn-gas generation while investigating operating conditions which more closely mimic industrial settings.

A key to the production of syn-gas from CO_2 is achieving the correct product selectivity. Previous work in the electrochemical reduction of CO_2 has largely focused on the conditions necessary to form different products including CO [4, 5] and a multitude of simple hydrocarbons such as methane [6, 7], ethylene [7, 8], carboxylic acids [9], and alcohols [10]. A key factor in determining the product distribution has been the cathode material [4, 11–13]. Metals that strongly adsorb CO (Pt group metals) and hydrogen tend to favor hydrogen evolution. Metals with weak CO adsorption and moderate hydrogen overvoltage (Ag, Au, Zn, and Cu) tend to form CO, although Cu electrodes primarily form hydrocarbons. Previous work has shown that Ag gas diffusion electrode (GDE) can be used to produce syn-gas [5]. In poorly catalytic metals (Hg,

E. J. Dufek · T. E. Lister (✉) · M. E. McIlwain
Idaho National Laboratory, P.O. Box 1625, Idaho Falls, ID 83415, USA
e-mail: tedd.lister@inl.gov

Cd, Pb, In, and Sn) formic acid is the primary product as C–O bonds are not broken without surface adsorption.

The second major technical challenge in the electrochemical reduction of CO_2 is the mass transport limitation associated with low CO_2 solubility in aqueous solutions. At planar metal electrodes, this results in relatively low current densities for CO_2 reduction. This has been improved through the incorporation of a GDE in the electrochemical cell [5, 8, 14, 15]. This report builds on previous work by incorporating a Ag GDE into a flow cell. This combination of cathode material, electrode type and cell design have been chosen to directly address issues with product selectivity and mass transport limitations in a system configuration similar to those used in industrial settings.

Cells for industrial alkaline water electrolysis operate at elevated temperatures (80–150 °C) due to heating associated with overpotentials and resistive losses [16]. To date investigations on the impact of temperatures above ambient on the electrochemical reduction of CO_2 have not been reported. This report aims to directly address this issue by increasing the temperature to more closely mimic expected industrial conditions in fully sized electrolyzers. As will be described, moderate increases in the cell temperature increase the overall cell efficiency by decreasing the kinetic overpotential (with slight thermodynamic decreases also observed [17]) for CO_2 reduction while maintaining the ability to produce CO and syn-gas. Thus, waste heat can be utilized to partially overcome these losses and improve cell efficiency. The effect of other important process variables such as CO_2 flow rate and current density are described and used to achieve specific syn-gas ratios for fuels production. It is envisioned that eventual scale up of this system may prove beneficial as a load-leveling technology or use with remote solar or wind energy projects. The investigations described precede a pilot-scale demonstration plant to generate syn-gas for fuels production.

2 Experimental

2.1 Electrochemical cell

As part of our long-term strategy for the production of syn-gas from CO_2 every attempt was made to ensure that the processes and cell components remained within the realm of commercial viability. For this reason, a commercially available filter-press type flow cell (Model AB, ElectroCell Systems) was modified in-house to incorporate a GDE (see Fig. 1). This cell design is highly scalable. Key advantages to the cell are the small anode to cathode spacing, the ability to effectively sweep gasses from the electrode surfaces and the promotion of mass transport to the electrode surface. In line with the long-term strategy a GDE containing a Ag catalyst (Silflon, Gaskatel) served as the cathode and an oxygen evolving, Ru-based dimensionally stable anode (DSA) was employed (ElectroCell Systems). An advantage to the use of commercial electrodes, especially the Ag GDE is that similar electrode systems are widely used in the chloro-alkali electrolysis industry as depolarizing electrodes [18]. Even after several years of use the specific electrode material chosen (Silflon) has shown minimal degradation in performance [19].

High purity CO_2 (Norco) was introduced to the back of the GDE using a manifold/current collector constructed of Type 304 stainless steel. The manifold had evenly spaced holes in a recessed area behind the active part of the electrode to promote even distribution of CO_2 to the back surface of the GDE while providing support to the electrode. Carbon dioxide flow into the back of the GDE was controlled using a mass-flow controller (1479A, MKS Inc.). Prior to introduction in the cell, CO_2 gas was passed through a hydrocarbon trap (Restek). Separation of the anode and cathode cell compartments was achieved using a Nafion® 424 cation exchange membrane. A salt bridge was used to provide contact between a Ag/AgCl (3 M NaCl) reference electrode (Bioanalytical Systems) and the cathode compartment. The cathode potentials are reported versus the Ag/AgCl reference. Mesh turbulence enhancers supplied with the flow cell were inserted in the open area of both flow plates. Each cell component was sealed via 0.16 mm thick Viton rubber. The anode and cathode active geometric areas were approximately 10 cm^2.

Both catholyte and anolyte solutions were cycled through the cell continuously during operation at flow rates of 30–40 mL min^{-1} using a multi-channel peristaltic pump and C-flex tubing (Masterflex-Cole Parmer). Flow of CO_2 through the GDE was initiated prior to flowing solutions into the cell. Solutions were enclosed in glass containers which were immersed in a water bath that was used to elevate the solution temperatures and subsequently the cell temperature. Prior to the start of experiments the temperature of the cell was allowed to stabilize. The temperature of the product stream at the outlet of the cathode compartment was monitored using a thermocouple which was in contact with the product stream. A LabVIEW (National Instruments)-based data acquisition system was used to capture the cell voltage and cathode potential. Polarization of the cell at a constant current was accomplished through the use of a DC power supply (30 V, 3 A, BK Precision).

2.2 Solutions

All chemicals used to make electrolyte solutions were ACS grade or better. Deionized water (18.2 MΩ cm) was used in the preparation of all solutions. Freshly prepared

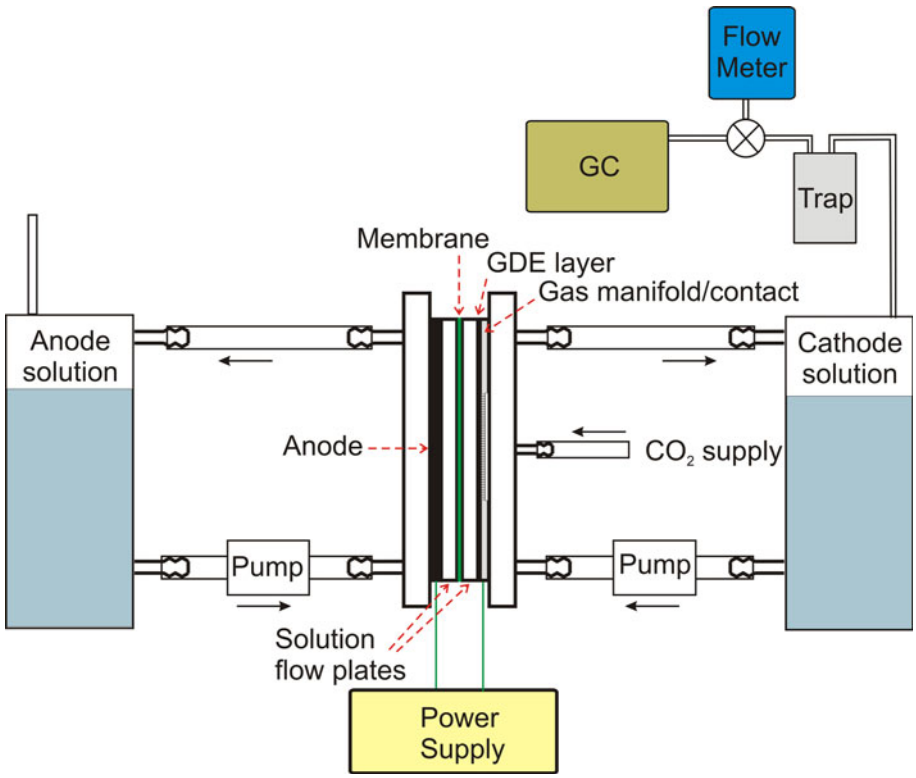

Fig. 1 Diagram of the electrolysis cell (see text for details)

solutions were used for each experimental run. Either 0.5 or 0.8 M K_2SO_4 was used as the catholyte and 2.5 M KOH served as the anolyte for all experiments. All materials contacting solution were thoroughly cleaned prior to use. The cell compartment was heated to 40 °C to prevent precipitation of catholyte for all experiments which used a 0.8 M K_2SO_4 catholyte solution.

2.3 Gas analysis

Head space analysis of the product gas for both the cathode and anode was accomplished using an injection loop on a gas chromatograph (GC) (Hewlett Packard 5890) equipped with thermal conductivity detectors. A manifold system directly passed the product gasses from the electrolyte headspace (usually the catholyte) through a water bath immersed in ice to the GC. The GC system was calibrated to determine percent gas composition for H_2, O_2, CO, and CO_2 analysis at the beginning of each day using mixtures of the above gases and N_2. For H_2, O_2, and CO analysis Ar carrier gas and an open tubular column (Molecular Sieve 5A, Hewlett Packard) was used. Carbon dioxide was determined using a CP PoraPLOT U capillary column (Varian, Inc.) using He carrier gas. Both columns were maintained at 150 °C during analysis. An Optiflow 520 (Supelco) digital bubble flow meter was used to determine the flow of product gas prior to each GC measurement. Formic acid analysis was performed on the cathode solutions (after acidification) using a GC (Model 6890, Hewlett Packard) equipped with a Nukol column (Supelco) and He carrier gas.

3 Results and discussion

The goal of this work was to build an electrolysis system based on available literature studies which operates in the most efficient and realistic manner. This entailed attaining the lowest cell voltage possible while operating at current densities similar to those used in the alkaline water electrolysis industry (100–200 mA cm^{-2}) [16]. Temperature was a focus because these systems typically operate at a minimum temperature of 80 °C due to heating associated with overpotential and cell resistance losses [16]. Ag cathodes were chosen due to their ability to produce CO from reduction of CO_2 [4, 5, 12, 20]. A GDE electrode was used to minimize mass transport issues associated with sparingly soluble CO_2 in aqueous solutions.

The role played by different electrolyte systems was not the main focus of this study, however, a few key considerations were used when choosing electrolytes. First, aqueous electrolytes were chosen due to issues associated with the oxidation of organic solvents (such as methanol) at the anode. Second, most aqueous based investigations of

CO_2 reduction have used bicarbonate-based electrolytes. For the present work, experiments were performed using either 0.5 or 0.8 M K_2SO_4 as the catholyte instead. Preliminary experiments showed little discernible difference in product selectivity between CO and H_2 with the use of bicarbonate or sulfate catholytes. Also, the sulfate system was chosen due to its higher conductivity (64 μS cm^{-1} for 0.5 M K_2SO_4 compared to 31 μS cm^{-1} for 0.5 M $KHCO_3$). Finally, $KHCO_3$ was not added to the catholyte due to the acid–base chemistry of CO_2 which, depending on pH, leads to the formation of CO_3^{2-} and HCO_3^-. The anolyte for all experiments was 2.5 M KOH. This is typical of the anolyte used for alkaline water electrolysis [16].

3.1 Effect of current density

Shown in Fig. 2a is a plot of cell voltage (E_{cell}) and cathode potential (E_c) during a current step experiment spanning 10–90 mA cm^{-2}. Carbon dioxide was delivered to the cathode at a flow rate of 20 mL min^{-1}. The measured backpressure was <0.5 psi. Starting at open circuit the current density (j) was first ramped to 10 mA cm^{-2} resulting in an increase in both E_{cell} and E_c. With each increase in j an increase in E_{cell} and E_c was observed. It should be noted that the noise of the measurements increased with j due to an increase in product gasses generated at the electrodes. At each current step, the system

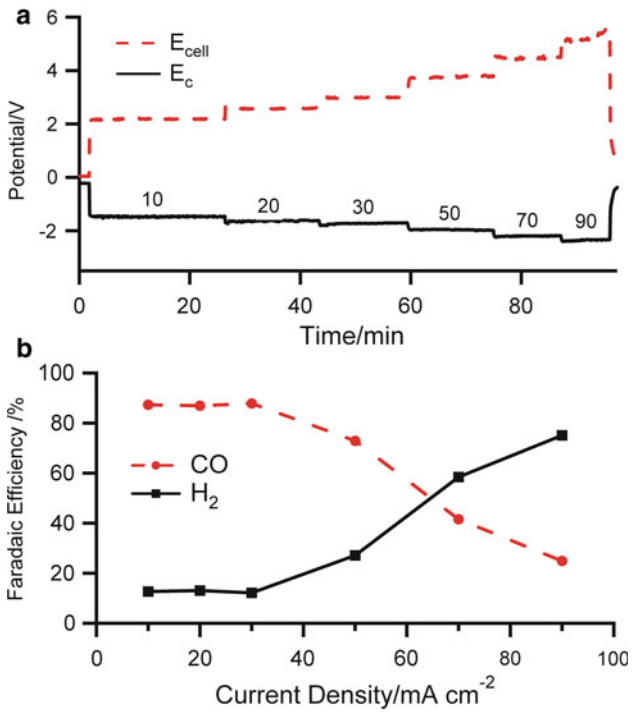

Fig. 2 Room temperature CO_2 reduction. CO_2 flow rate 20 mL min^{-1} **a** E_{cell} and E_c, **b** FE for the production of CO and H_2

was stable with little variance until 90 mA cm^{-2}. At 90 mA cm^{-2}, following the initial increase, E_{cell} rapidly increases while E_c remains stable. The rapid increase in E_{cell} is attributed to partial blockage of the membrane by precipitated catholyte. While the initial concentration of catholyte is below the room temperature solubility of ~0.6 M for K_2SO_4 [20], the movement of K^+ from the anolyte to the catholyte over the course of the experiment results in a sufficiently high concentration to initiate localized precipitation of K_2SO_4 near the membrane causing an increase in the cell impedance. This was confirmed by observation of precipitated salt on the cathode side of the membrane.

In conjunction with monitoring E_{cell} and E_c, analysis of the product stream was performed. Displayed in Fig. 2b are the Faradaic efficiencies (FE in %) calculated from the analysis of the cathode product stream for CO and H_2 at each of the j values investigated in Fig. 2a. To calculate FE the moles produced in 1 min of cell operation were determined from the density of each individual gas, the flow rate of the product stream and the percent gas composition. This value in conjunction with the charge passed for 1 min of operation at a given current was used to arrive at the final FE values. As the current increased the FE associated with the production of CO remained near 90% from 10 to 30 mA cm^{-2}. Above 30 mA cm^{-2} the CO FE drops to the point where at 90 mA cm^{-2} it is near 25%. It should be pointed out that while the FE remains nearly level between 10 and 30 mA cm^{-2} the total amount of CO generated increases as the current increases. The FE for H_2 follows the opposite trend of CO where at low j values low FE values are seen with the percentage increasing as j is increased. It should be noted that formic acid was not detected in the catholyte solution at the completion of experiments. This is not entirely unexpected as the FE for formic acid from another report was below 2% [5].

The data from Fig. 2 provides a baseline from which the current bench-scale cell can be compared to previous reports. Comparing the cell performance to previous work by Newman et al. where a buffer layer cell incorporating a Ag GDE was used, it can be seen that at low j similar values are observed for E_{cell} and E_c [5]. At high j values, E_{cell} increases above the levels in the previous report. The FE of the two data sets is comparable at similar run times for both systems. A second similar system for comparison was reported by Hori et al. where Ag was deposited on either a cation or anion exchange membrane [21]. For the anion exchange membrane at the lower j shows lower E_c values and similar FE for the generation of CO, while at the higher j the E_c values are above this report but have greater FE for CO generation. Thus, it was deemed that the system at room temperature is comparable to previous reports.

3.2 Effect of temperature

Following establishment of a performance baseline for the cell a set of experiments investigating the influence of increasing the temperature was performed. This was intended to determine possible effects of cell heating normally observed in commercial scale electrolysis stacks which typically operate at 80–150 °C [16]. The results of these experiments can be seen in Figs. 3 (cell and cathode voltages) and 4 (product data). As can be seen in Fig. 3 increasing the temperature has a profound influence on both E_{cell} and E_c. At 70 mA cm^{-2} E_{cell} drops by 1.57 V from 4.45 V at 18 °C (room temperature operation) to 2.88 V at 70 °C (boiling water bath). In conjunction with the decrease in E_{cell} a drop in E_c from −2.19 to −1.87 V for the same temperatures is observed. The decrease in E_{cell} can be attributed to several contributions. First, the potential at the cathode increased by 0.32 V. The remainder of the drop in cell voltage must then be associated with a decrease in the anode potential and a drop in the impedance associated with the electrolyte and membrane. Electrolyte conductivity should increase with temperature and product gas bubbles become smaller leading to less shielding of the electrodes and electrolyte. A key implication of these changes is that the j window where E_{cell} remains below 4 V increases by close to 100 mA cm^{-2} at 70 °C. This puts the cell at the lower end of the j range used in commercial alkaline water electrolysis operations albeit at higher cell voltages [16].

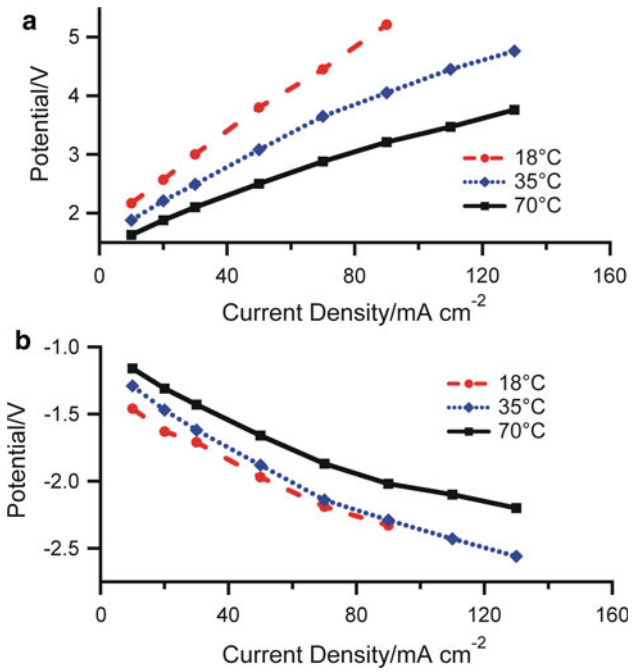

Fig. 3 Cell performance at 18, 35, and 70 °C, CO_2 flow 20 mL min^{-1} **a** E_{cell} and **b** E_c

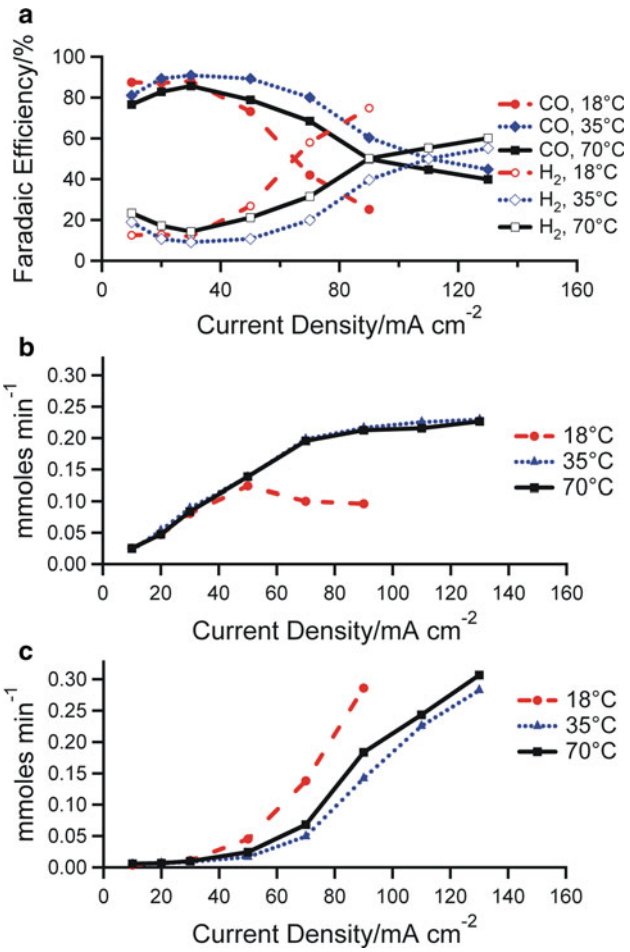

Fig. 4 Cell performance at 18, 35, and 70 °C, CO_2 flow 20 mL min^{-1} **a** FE for CO and H_2 **b** mmoles min^{-1} of CO produced, and **c** mmoles min^{-1} H_2 produced

Both thermodynamic and kinetic parameters dictate the potential where H_2 and CO are evolved at the cathode. At room temperature a key limitation to CO_2 reduction is the large kinetic overpotential needed for the production of CO. As shown above, the potentials decrease considerably as the temperature of the cell is increased. Using thermodynamic data it is possible to calculate the thermodynamic change in potential for both CO_2 and H_2O reduction as the temperature is increased [17]. Calculations show a decrease of <0.1 V is predicted for the reduction potentials for both cathodic reactions when changing the temperature from 25 to 125 °C (the next lowest temperature where thermodynamic data was available). This accounts for only a portion of the observed decrease in E_c suggesting that a more profound driving force for the decrease in E_c is the decrease in the overpotential needed to drive the reactions.

While a decrease in E_{cell} is valuable, the product distribution at the different j values is also important in evaluating the full cell performance. The FE for CO and H_2 and the moles of CO and H_2 produced per minute can be

seen in Fig. 4. As with the data presented in Fig. 3 a discernible change is seen as the cell temperature is increased from room temperature. Most dramatic is that the j range where the FE for CO remains above 75% is increased to 70 mA cm^{-2} for the intermediate temperature (35 °C) and 50 mA cm^{-2} for 70 °C. Below these j values there is little difference in the FE for the different temperatures. Above these values, the CO FE for the higher temperatures are all well above that of the room temperature cell operation. An interesting observation from Fig. 4a is that the j where the FE for H_2 crosses over that of CO is at a maximum at 35 °C but then decreases at 70 °C. This could be related to the decrease in solubility of CO_2 with temperature creating a mass transport limitation or hint that the overpotential for H_2O reduction is influenced more than the overpotential for reduction of CO_2.

While FE for the products provides information on the product distribution being generated at the cathode, it gives little information on the amount of CO produced. In Fig. 4b and c, the experimentally determined production rates of CO and H_2 are presented. As can be seen, at low j values there is again little if any difference in the total CO produced. Above 50 mA cm^{-2} the CO produced increases for the higher temperature runs while the total amount decreases for the room temperature experiment. At the elevated temperatures above 90 mA cm^{-2} the amount of CO plateaus near 2.2×10^{-4} mol min^{-1}. This plateau is likely associated with limited mass transport of CO_2 to the cathode at this particular flow rate. The production of H_2 remains low for all temperatures until 50 mA cm^{-2}. Above that point the amount of H_2 generated at the cathode increases. While some variance in H_2 production is seen it is less dramatic than that observed for CO. The production levels for CO are especially promising. As expected the use of the Ag GDE helps balance out concerns with the solubility of CO_2 at elevated temperature. This is significant as the solubility of CO_2 in K_2SO_4 decreases by close to a factor of 4 between 25 and 75 °C [22].

Using the FE and the E_{cell} the overall cell efficiency can be determined [5]. The calculated values are shown in Fig. 5 where cell efficiency decreases with increasing current density. This trend closely follows previously reported values for full cell analysis of CO_2 reduction [5]. The key is that by increasing the cell temperature the cell efficiency increases for all the currents investigated. At 70 mA cm^{-2} the increase in cell efficiency from room temperature to 70 °C is 18%. This increase in efficiency is directly related to the decreases seen in the E_{cell} values. It is recognized that this method of calculating the cell efficiency ignores the energy required in heating the cell. However, commercial scale electrolysis cells are designed to use current-resistance losses to heat the cell resulting in improved efficiency.

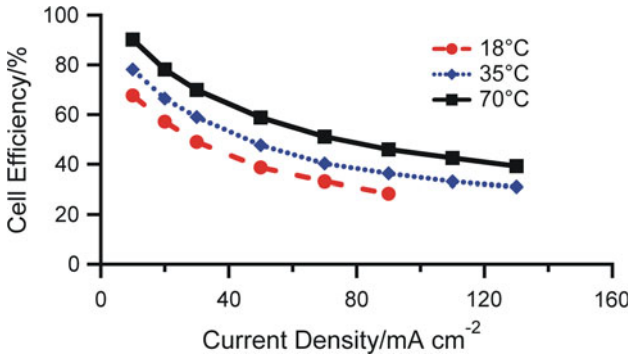

Fig. 5 Cell efficiency at 18, 35, and 70 °C, CO_2 flow 20 mL min^{-1}, 0.5 M K_2SO_4 catholyte

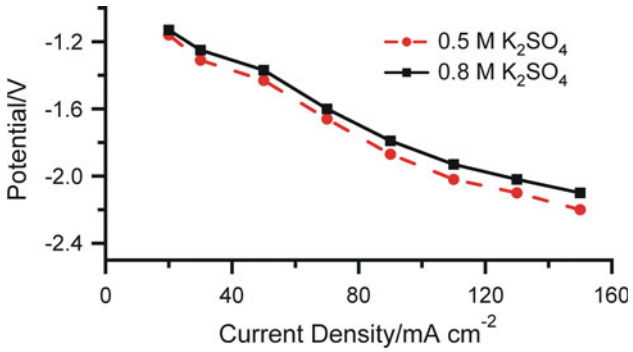

Fig. 6 Influence of catholyte concentration, 70 °C, CO_2 flow 20 mL min^{-1}

3.3 Effect of catholyte concentration and CO_2 flow rate

Recall that in Fig. 2 a dramatic increase in E_{cell} was observed at 90 mA cm^{-2}. This increase was attributed to the localized precipitation of catholyte near the membrane. Increasing cell temperature alleviates this issue as the solubility of K_2SO_4 increases from ~0.6 M at room temperature to above 1.2 M at 70 °C [20]. In addition to mitigating issues with catholyte precipitation, increasing the cell temperature makes it possible to increase the concentration of the catholyte. A comparison of 0.5 M and 0.8 M K_2SO_4 as the catholyte at 70 °C with a CO_2 flow rate of 20 mL min^{-1} is shown in Fig. 6. At 0.8 M the concentration of catholyte is below the solubility limit, yet still sufficiently high to produce an increase in conductivity to 137 μS cm^{-1}. Shown in Fig. 6 are the E_c values for the two catholyte systems. As expected the increase in conductivity lowers the E_c values at the greater of the two catholyte concentrations.

Optimal production of secondary chemicals from syngas requires the correct H_2:CO ratio. Ideally for methanol production a ratio of 2:1 is desired [1]. For dimethyl ether (DME), a possible replacement for diesel fuel, production using a mixed catalyst performs best with a ratio between

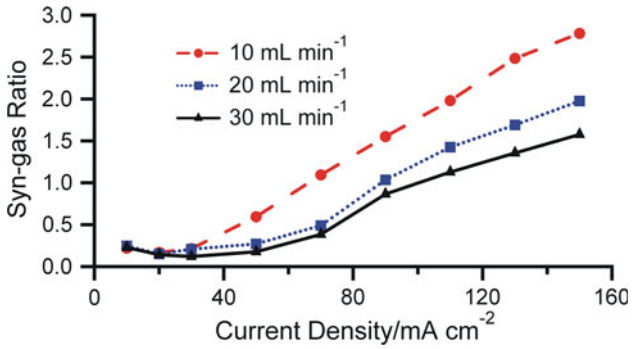

Fig. 7 Syn-gas (H_2:CO) ratio as a function of CO_2 flow rate, 0.8 M K_2SO_4 catholyte, 70 °C

1 and 1.5:1 [1, 23–25]. From Fig. 4, the H_2:CO ratio varies from 0.25 to 1.98:1 when moving from 10 to 150 mA cm^{-2} at 70 °C. Thus, only at the highest j value investigated is the ideal ratio for methanol production met. However, as shown in Fig. 4b, there is a mass transport limitation above 90 mA cm^{-2} which results in a plateau in the amount of CO produced. Thus, another means to increase the H_2:CO ratio is to reduce the flow of CO_2 to the cathode. Figure 7 contains the data from a set of experiments where the CO_2 flow rate was varied between 10 and 30 mL min^{-1}. Due to the slight increase in performance described above these experiments were conducted using 0.8 M K_2SO_4 catholyte. As can be seen, limiting the amount of CO_2 available to reach the electrode surface results in a increase in the H_2:CO ratio. While the ratio increases there is little if any change in either E_{cell} or E_c for a set current density. Therefore, by restricting the flow of CO_2, the ability to produce syn-gas at the correct composition for the eventual formation of methanol is possible at lower current densities and cell voltages.

An implication of decreasing the CO_2 flow rate is the subsequent decrease in the amount of syn-gas produced and the possibility that despite lower currents and E_{cell} values, the energy required to generate equal amounts of syn-gas may actually increase. The variance in the energy needed for production of a kilogram of syn-gas with different H_2:CO ratios is shown in Table 1. It becomes clear from this data that controlling the flow of CO_2 can be used to tailor syn-gas composition without sacrificing the production scale. For the present set of conditions, generation of syn-gas for the production of DME is optimized with a flow rate of 30 mL min^{-1} while a flow rate of 10 mL min^{-1} is more suited for generation of syn-gas for methanol production.

The reproducibility of syn-gas production is important to the eventual scale up of the current bench-scale system. Using two independent GDE electrodes the experimental reproducibility was evaluated using a minimum of four data points per j value. Each run involved increasing the

Table 1 Energy required to produce a kg of syn-gas at different CO_2 flow rates

Flow rate (mL min^{-1})	Syn-gas ratio	kW h kg^{-1} Syn-gas
10.0	1.09	8.87
10.0	1.55	11.5
10.0	1.98	14.0
20.0	1.13	9.63
20.0	1.35	11.5
20.0	1.58	14.1
30.0	1.04	8.31
30.0	1.43	10.3
30.0	1.98	14.8

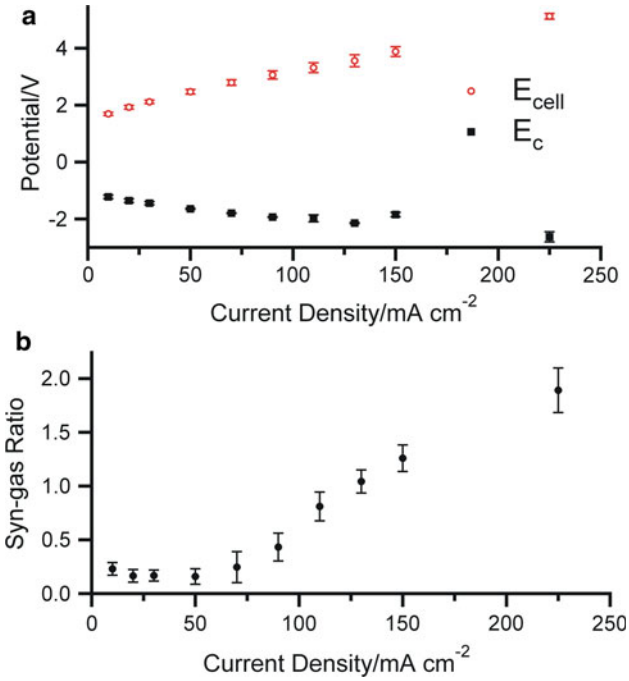

Fig. 8 System reproducibility, **a** E_c and E_{cell}, **b** Syn-gas (H_2:CO) ratio, 70 °C, CO_2 flow 30 mL min^{-1}

current density in a manner similar to that in Fig. 2 at 70 °C using 0.8 M K_2SO_4 as the catholyte and a CO_2 flow rate of 30 mL min^{-1}. Presented in Fig. 8a are the E_{cell} and E_c values while Fig. 8b contains the data for the H_2:CO syn-gas ratio. The data in Fig. 8 clearly display that the system is reproducible both in terms of the potentials necessary for CO_2 reduction, but also in its ability to produce a specified composition of syn-gas.

3.4 Production of syn-gas and cell stability

Thus far the experiments described have focused on cell performance for the production of CO and H_2 over relatively short periods of time. Elevating the temperature to

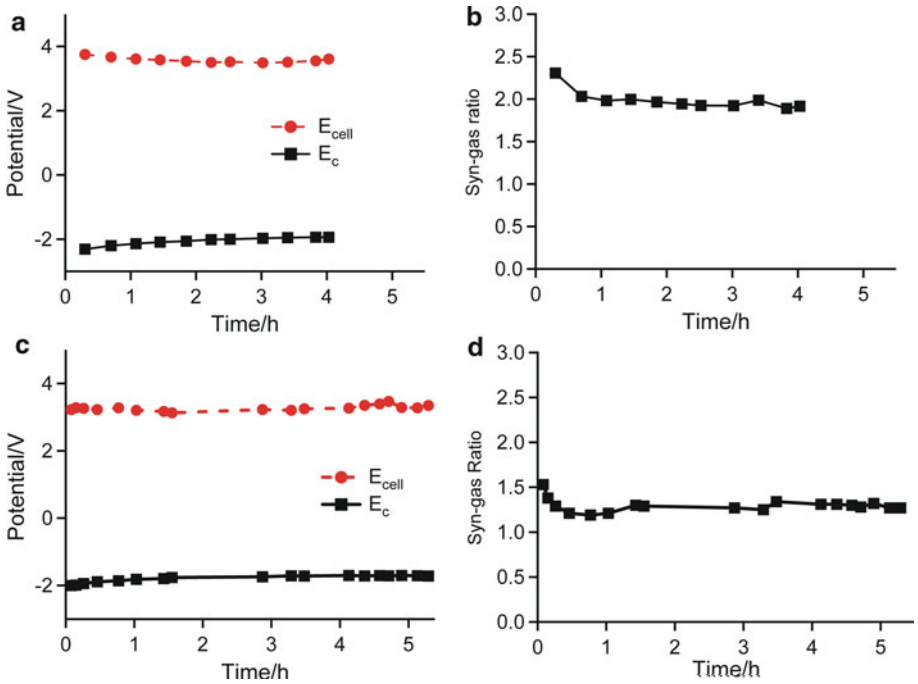

Fig. 9 Generation of syn-gas mixtures at 70 °C in 0.8 M K_2SO_4 catholyte. **a**, **b** Methanol mixture: CO_2 flow 10 mL min^{-1} and 117.8 mA cm^{-2}, **c**, **d** DME mixture: CO_2 flow of 30 mL min^{-1} and 95 mA cm^{-2}

70 °C proves valuable in increasing the cell efficiency and providing a means to reproducibly generate syn-gas. Thus, longer runs performed under static conditions were performed. In Fig. 9a and b, the cell performance for a run where the j was held at 117.8 mA cm^{-2} with a CO_2 flow rate of 10 mL min^{-1} are shown. These conditions are roughly what would be necessary to produce a syn-gas H_2:CO ratio of 2. For the first 30 min of cell operation after the initial application of current both E_{cell} and E_c gradually decrease before stabilizing for the remainder of the 4 h run. At the very end of the run a slight increase in E_{cell} is most likely associated with the consumption of OH^- in the anolyte. For this run no additional base was added to the anolyte to compensate for depletion associated with oxygen evolution. We plan on devising means to mitigate this issue in future work. In Fig. 9c and d, the j was held at 95 mA cm^{-2} with a CO_2 flow rate of 30 mL min^{-1} to mimic the conditions necessary to produce syn-gas for DME production. In a manner similar to Fig. 9a following an initial decrease in the H_2:CO ratio the system stabilized for the remainder of the experiment. Due to the decreased j the cell life for the lower H_2:CO ratio is increased because less OH^- is consumed at the anode per unit time.

The evolution of E_{cell} and E_c indicate the conditions within the cell are changing during the initial cell operation for both experiments. To investigate if the change was related to electrode poisoning the system was flushed with water and fresh catholyte and anolyte solutions were introduced to the cell. Again long-term experiments were performed. For each experiment, including experiments at different j values from the two shown above, similar behavior was seen. For this reason, we attribute the decrease in E_{cell} and E_c to be the result of the evolution of the catholyte composition. In Fig. 9a, the plateau in the E_c occurs after slightly <1 h of cell operation. Calculations indicate that in the first 40 min of cell operation, based on the rates of H_2 and CO production for the conditions in Fig. 9a, the catholyte solution evolves from a pH of 6.5 and low levels of carbonate to a pH of near 13.5 (0.12 M OH^-) and a concentration of CO_3^{2-} of just over 0.11 M. A solution consisting of these components in addition to the 0.8 M K_2SO_4 has a conductivity of 155 μS cm^{-1} at 70 °C or a roughly 13% increase in conductivity over the initial catholyte at the same temperature. At the completion of a 4 h electrolysis experiment the conductivity of the catholyte measured 149 μS cm^{-1} indicating that despite continued increases in the pH due to OH^- production little additional change in the conductivity of the catholyte occurs. As a consequence of the decrease in E_c the composition of the product gas is altered where at lower E_c values the production of CO is favored over H_2 resulting in lower H_2:CO syn-gas ratios. Once E_c has stabilized little observed change in the syn-gas ratio occurs.

A possible complication of the present cell design is the crossover of H_2 from the cathode side of the cell through the membrane to the anode. During long-term experiments both the cathode and anode product gasses were collected in parallel. The cathode gas composition has been discussed thoroughly above. At the anode the oxidation of water to O_2 occurs, thus the anode product gas should

consist of entirely O_2 if little crossover of H_2 from the cathode to the anode compartments occurs. Analysis of the gas from the anode compartment reveals that only minimal H_2 is present. Even at j values up to 225 mA cm^{-2}, where the predominant cathode gas is H_2, only 0.06% of the product gas collected from the anode is H_2. This accounts for <0.05% of the H_2 produced at the cathode. The balance of the gas was O_2.

4 Conclusions

Elevating the temperature at which the electrochemical reduction of CO_2 occurs to levels commonly seen in industrial cells provides promise as a first step in making the present system a viable load-leveling technology. It has been demonstrated that by increasing the temperature of a cell equipped with a Ag GDE from room temperature to 70 °C results in an E_{cell} decrease of 1.57 V at 70 mA cm^{-2}. The decrease in E_{cell} can be attributed to both the anode and cathode potentials. On the cathode side the increase arises primarily from decreasing the kinetic overpotential necessary for the reductions of CO_2 and H_2O. The respective products of these two reductions can be tightly controlled by altering the CO_2 flow rate and the cell j enabling the generation of syn-gas which meets the requirements for the production of either DME or methanol. In addition, the working window for the cell increases with temperature by over 100 mA cm^{-2}. Cell performance has been shown to be reproducible with minimal crossover of H_2 from the cathode compartment to the anode. Finally, the evolution of the composition of the catholyte initially plays a key role in the ratio of products, however, after an initial period the product composition remains stable.

Acknowledgments Work supported through the INL Laboratory Directed Research & Development (LDRD) Program under DOE Idaho Operations Office Contract DE-AC07-05ID14517.

References

1. Olah G, Goeppert A, Prakash GKS et al (2006) Beyond oil and gas: the methanol economy. Wiley-VCH, Weinheim
2. Jitaru M, Lowry DA, Toma M et al (1997) J Appl Electrochem 27:875
3. Gattrell M, Gupta N, Co A (2007) Energy Convers Manag 48:1255
4. Hara K, Kudo A, Sakata T (1995) J Electroanal Chem 391:141
5. Delacourt C, Ridgway PL, Kerr JB et al (2008) J Electrochem Soc 155:B42
6. Hara K, Sakata T (1997) J Electrochem Soc 144:539
7. Hara K, Tsuneto A, Kudo A et al (1997) J Electroanal Chem 434:239
8. Cook RL, Macduff RC, Sammells AF (1990) J Electrochem Soc 137:607
9. Whipple DT, Finke EC, Kenis PJ (2010) Electrochem Solid State Lett 13:B109
10. Frese KW, Leach S (1985) J Electrochem Soc 132:259
11. Azuma M, Hashimoto K, Hiramoto M et al (1989) J Electroanal Chem 260:441
12. Hori Y, Wakebe H, Tsukamoto T et al (1994) Electrochim Acta 39:1833
13. Azuma M, Hashimoto K, Hiramoto M et al (1990) J Electrochem Soc 137:1772
14. Mahmood MN, Masheder D, Harty CJ (1987) J Appl Electrochem 17:1223
15. Yamamoto T, Tryk DA, Hashimoto K et al (2000) J Electrochem Soc 147:3393
16. Stolten D, Krieg D (2010) In: Stolten D (ed) Hydrogen and fuel cells. Wiley-VCH, Weinheim
17. Chase MWJ (1998) NIST-JANAF thermochemical tables, 4th edn. Journal of Physical Chemistry Refence Data. http://webbook.nist.gov/chemistry/form-ser.html. Accessed October 2010
18. Moussallem I, Jorissen J, Kung U et al (2008) J Appl Electrochem 38:1177
19. Tetzlaff KH, Walz R, Gossen CA (1994) J Power Sources 50:311
20. Phillips JGE (2005) 3.2 Properties of inorganic compounds. http://www.kayelaby.npl.co.uk. Accessed February 2011
21. Hori Y, Ito H, Okano K et al (2003) Electrochim Acta 48:2651
22. He SL, Morse JW (1993) Geochim Cosmochim Acta 57:3533
23. Moradi GR, Ghanei R, Yaripour F (2007) Int J Chem React Eng 5:1542
24. Moradi G, Ahmadpour J, Nazari M et al (2008) Ind Eng Chem Res 47:7672
25. Fujimoto K, Asami K, Shikada T et al (1984) Chem Lett 12:2051